

COMMUNICATION

CrossMark
click for updatesCite this: *Dalton Trans.*, 2016, **45**,
12301Received 24th June 2016,
Accepted 13th July 2016

DOI: 10.1039/c6dt02538b

www.rsc.org/dalton

A Mn(III) single ion magnet with tridentate
Schiff-base ligands†S. Realista,^a A. J. Fitzpatrick,^b G. Santos,^a L. P. Ferreira,^{c,d} S. Barroso,^e L. C. J. Pereira,^f
N. A. G. Bandeira,^{a,e,g} P. Neugebauer,^h J. Hrubý,^h G. G. Morgan,^b J. van Slageren,^h
M. J. Calhorda^a and P. N. Martinho*^a

Single ion magnet behaviour is reported for a mononuclear Mn(III) ion with tridentate Schiff-base ligands which exhibits a tetragonal Jahn–Teller elongation along the $N_{\text{amine}}\text{--Mn--}N_{\text{amine}}$ axis and crystallises with two crystallographically distinct Mn(III) cations (unit A and unit B). While magnetic measurements show a large and negative axial zero-field splitting ($D = -4.73 \text{ cm}^{-1}$), HF-EPR reveal two distinct large axial D s ($D = -4.60 \text{ cm}^{-1}$ for unit A and $D = -4.18 \text{ cm}^{-1}$ for unit B), thus resulting in the largest D known to date for a Mn(III) single ion magnet. AC magnetic measurements at 2000 Oe allowed determination of the energy barrier for spin reversal (10.19 K) and spin reversal relaxation time ($1.476 \times 10^{-6} \text{ s}$) for the Mn(III) ion. Computational studies were used to characterise the electronic structure and substantiate the zero field splitting in the Mn(III) complex.

Introduction

Magnetic properties have traditionally been associated with infinite solids, such as bulk metals, or, not so long ago, infinite inorganic polymeric solids of variable dimensionality. The observation, in 1993, by Sessoli *et al.*,¹ that a discrete mixed-

valence cluster containing twelve manganese centers, $[\text{Mn}_{12}\text{O}_{12}(\text{CH}_3\text{CO}_2)(\text{H}_2\text{O})_4]\cdot 4\text{H}_2\text{O}\cdot 2\text{CH}_3\text{CO}_2\text{H}$ (Mn12ac), exhibited slow magnetic relaxation in the absence of a magnetic field, opened the way to species that became known as single molecule magnets (SMMs). Their relevance in the development of more miniaturised high-density magnetic memory and other devices was immediate.² Upon magnetisation, the unpaired spins align in a preferential direction and at low temperature the magnetisation is retained for some time after removal of the magnetic field.² The next step in the search for new materials consisted of moving from clusters to mononuclear complexes of d or f elements with unpaired electrons. This was achieved, after a few years of effort, when Long reported in 2010³ the first example of slow magnetic relaxation observed in a high spin 3d transition metal, Fe(II). The term single ion magnets (SIMs) was coined to describe these new materials. Since then, the examples of 3d SIMs have been extended to other complexes of Fe(II) and other centers, such as Fe(I), Fe(III), Co(II), Mn(III), Ni(I) and Ni(II).^{4–10} The slow magnetic relaxation is associated with a barrier (U_{eff}), which depends on the uniaxial magnetic anisotropy (D) and the total ground state spin (S_{T}) according to $U_{\text{eff}} = |D|S_{\text{T}}^2$,² and the higher the barrier the better. The most obvious way to increase U_{eff} is to choose an electronic configuration that maximises the number of unpaired electrons (higher S_{T}). The trend from infinite solids to clusters and to mononuclear complexes goes exactly in the opposite way, explaining why it was not so easy to find SIMs. High spin complexes will be possible for $3d^4$ to $3d^7$ electron configurations, as long as the metal–ligand interaction remains relatively weak (low charge on the metal, weak ligands). In recent years monometallic lanthanide complexes have also emerged as a class of SIMs with high barriers.¹¹ Increasing the D value is the alternative, but it is limited by the fact that D and S_{T} are not independent and D values generally decrease with increasing S_{T} .^{12,13} The barrier in Long's $3d^6$ Fe(II) tetra-coordinate complex is $U_{\text{eff}} = 42 \text{ cm}^{-1}$. Octahedral $3d^4$ Mn(III) complexes have the same S_{T} , but are tetragonally distorted (usually elongated) owing to the Jahn–Teller effect.¹⁴ The ^5E ground state splits into $^5\text{A}_1$ and $^5\text{B}_1$, leading to mixing

^aCentro de Química e Bioquímica, Faculdade de Ciências, Universidade de Lisboa, Campo Grande, 1749-016 Lisboa, Portugal. E-mail: pnmartinho@ciencias.ulisboa.pt

^bSchool of Chemistry, University College Dublin, Belfield, Dublin 4, Ireland

^cBioISI, Faculdade de Ciências, Universidade de Lisboa, Campo Grande, 1749-016 Lisboa, Portugal

^dDepartment of Physics, University of Coimbra, 3004-516 Coimbra, Portugal

^eCentro de Química Estrutural, Instituto Superior Técnico, Universidade de Lisboa, Av. Rovisco Pais, 1049-001 Lisboa, Portugal

^fC2TN, Centro de Ciências e Tecnologias Nucleares, Instituto Superior Técnico, Universidade de Lisboa, Estrada Nacional 10, ao Km 139, 7, 2695-066 Bobadela LRS, Portugal

^gInstitute of Chemical Research of Catalonia (ICIQ), Avda. Països Catalans, 16-43007 Tarragona, Spain

^hInstitut für Physikalische Chemie, Universität Stuttgart, Pfaffenwaldring 55, 70569 Stuttgart, Germany

† Electronic supplementary information (ESI) available: Structural data, magnetic data, HF-EPR data and computational data. CCDC 1451873. For ESI and crystallographic data in CIF or other electronic format see DOI: 10.1039/c6dt02538b

meter, g is the average g -factor, μ_B is the Bohr magneton, and B is the magnetic field. Fitting of the data gives axial (D) and transverse (E) zero field splitting parameters of -4.73 cm^{-1} and 0.09 cm^{-1} , respectively with $g = 1.988$. The relationship between D and E is interesting as the small $|E/D|$ ratio gives insight into the predominant anisotropy, axial, which is associated with the axial Jahn–Teller elongation in complex **1**.

In order to better estimate the spin Hamiltonian parameters g , D and E we performed high frequency-EPR measurements. The obtained spectra are shown in Fig. 3 and S3.† The fact that the absorption-shaped parallel features are located at low fields, while derivative-shaped perpendicular features are located at high fields immediately suggests a negative sign for the D -parameter. Furthermore the zero field crossing at about 300 GHz suggests a magnitude of D around 3.3 cm^{-1} . Simulations of the spectra according to the spin Hamiltonian (eqn (1)) revealed the presence of two species in a one to one ratio in accordance with the crystallographic data which will hereinafter be referred to as units A and B. Table 1 lists the obtained parameter values.

The size of the axial anisotropy is higher than the previously published examples of tetragonally elongated Mn(III)

ions, ranging from -3.2 to -3.9 cm^{-1} .^{8,19–22} Dynamic magnetic measurements were then undertaken to investigate whether any slow relaxation of the magnetisation occurred in complex **1**, as complexes with similar axial anisotropy values have been found to exhibit field induced slow relaxation. Under a zero DC field (Fig. S5a and b†) there is no evidence of slow relaxation on the temperature dependence of the AC susceptibility, neither for the real component of the susceptibility, χ'_m , nor for the out-of-phase component, χ''_m . This result is typical of mononuclear Mn(III) complexes that exhibit SIM behaviour known to date and is related to the quantum tunnelling of the magnetisation, through the thermal relaxation barrier, between the $m_s = 2$ and $m_s = -2$ states. This is the dominant relaxation pathway and as such makes it impossible for the magnetisation barrier to block the reorientation of a spin. The very small ratio of $|E/D|$ allows this relaxation by the overlapping of the m_s states.^{25,26}

However, application of a DC field should split the m_s levels and inhibit the quantum tunnelling pathway and/or spin–spin relaxation. Under an applied DC field of 2000 Oe, very clear out-of-phase, χ''_m , signals are observed, Fig. 4. The data exhibits clear maximum values in the χ''_m response. At these maximum values the angular frequency, ω , can be related to the relaxation time, τ , and the rate of relaxation at a particular frequency can be derived using:

$$\omega\tau = 2\pi \frac{1}{\tau} = 1 \quad (2)$$

The magnetisation relaxation rate was then evaluated at these fixed temperatures while the frequency, ω , of the AC field was varied from 10 Hz to 10 kHz providing data for the Cole–Cole plots (χ''_m vs. χ'_m) that were in turn fitted to obtain the τ values (see details in ESI Fig. S6a†). The relationship

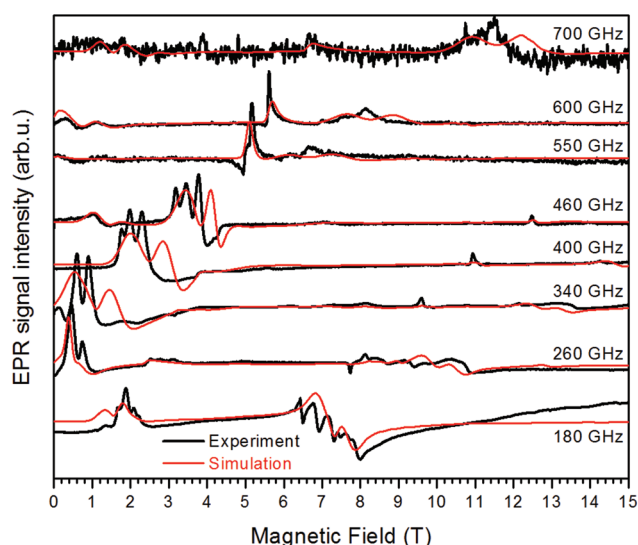


Fig. 3 High frequency EPR spectra (in black) of compressed powder recorded at 5 K at the frequencies indicated in the plot, together with simulation (in red) obtained using parameters indicated in Table 1.

Table 1 Spin Hamiltonian parameters extracted from HF-EPR spectra

Crystallographic unit A		
D/cm^{-1}	-4.60	± 0.05
E/cm^{-1}	1.5	± 0.05
g_{iso}	1.987	± 0.015
Crystallographic unit B		
D/cm^{-1}	-4.18	± 0.05
E/cm^{-1}	1.5	± 0.10
g_{iso}	1.987	± 0.015

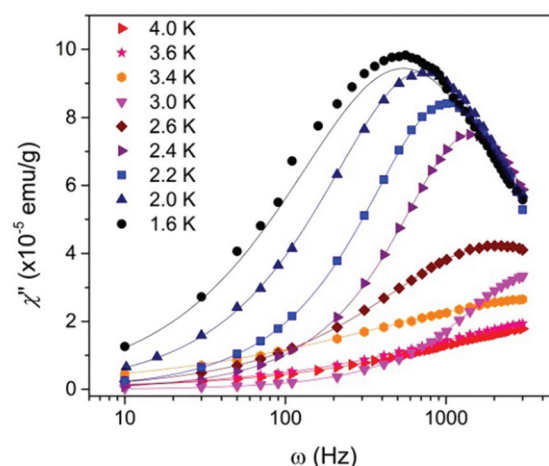


Fig. 4 Frequency dependence of the out of phase susceptibility, χ''_m , for complex **1**, under a static DC field of 2000 Oe with a 2 Oe oscillating field in the range 1.6–4 K. The lines represent the least-squares fits with a generalized Debye model to a distribution of single relaxation modes (see ESI†).

between the relaxation time and temperature can be investigated through an Arrhenius plot of $\ln(\tau)$ vs. $1/T$, Fig. S6b,† according to the equation:

$$\ln \tau = \ln \tau_0 + U_{\text{eff}}/k_{\text{B}}T \quad (3)$$

Therefore the effective barrier for reversal of the magnetisation, U_{eff} , and the relaxation attempt time for reversal for $T = \infty$, τ_0 , can be estimated. From this fit, values of $U_{\text{eff}} = 10.19$ K (7.08 cm^{-1}) and $\tau_0 = 1.476 \times 10^{-6}$ s were obtained (Fig. S6b†).

A computational analysis was performed on the two asymmetric crystallographic units to characterise their electronic structure and reproduce the zero field splitting (see ESI†). The initial approach used the CASSCF state interaction spin-orbit coupling (CASSCF + SOC) formalism (RASSI module) in MOLCAS as it has successfully been used to compute the ZFS parameters.^{27–30}

The D and E parameters are frequently calculated at the CASSCF level.³¹ ZFS is essentially a local phenomenon, thus it is sufficient to take only into account the full correlation within the 3d orbitals to yield values with reasonable accuracy. The smallest active space was chosen incorporating the four electrons in the five d orbitals of Mn(III). The calculated values are listed on the left-hand side of Table 2 (see also ESI†). Their disappointing underestimation in comparison to the values obtained from both magnetic and HF-EPR measurements prompted us to improve the computational method for better evaluation. While the singlet states play only a very residual role in the SOC ground state multiplet, the triplet states are essential to describe the five initial SOC states. The energy eigenvalues of each multiplet component resulting from the (MOLCAS) CASSCF + SOC run are 0.0, +0.40, +8.13, +12.00, and +13.67 cm^{-1} each with 99.87%, 99.87%, 99.92%, 99.94% and 99.95% contribution respectively from the X^5A spin-free state.

A more reliable option can be found with the NEVPT2 method³² implemented in the ORCA program. By using the Dyal Hamiltonian the intruder state problem can be eschewed and the perturbation procedure does not require iterative steps. The results for both units A and B are listed on the right-hand side of Table 2. The NEVPT2 D and E values from ORCA are an improvement on those resulting from the CASSCF (MOLCAS) calculations. The inclusion of correlation through NEVPT2 + SOC improves both the axial and the rhombic anisotropy. This trend is consistent with the previous

work of Duboc *et al.*³¹ where the perturbation correction decreases the energies of the interacting states, allowing for a greater admixing, and consequently an increase in the absolute values of D and E .

The most significant contributor to the axial anisotropy (D) is the lowest energy triplet which contributes -0.949 cm^{-1} (CASSCF) or -1.631 cm^{-1} (NEVPT2) to the overall tensor. This triplet state has a dominant $3d_{xy}^1 3d_{yz}^1 3d_{xz}^2 3d_{z^2}^0 3d_{x^2-y^2}^0$ configuration (87.9%), which corresponds to doubly filling the d orbital bisecting the plane of the nitrogen donor ligands. Recall that the ground state quintet has the $3d_{xy}^1 3d_{yz}^1 3d_{xz}^1 3d_{z^2}^1 3d_{x^2-y^2}^0$ configuration where relieving the Mn–N anti-bonding interaction between the occupied $3d_{z^2}$ orbital with the nitrogen donor ligands causes the structural distortion.

To discard the possibility that the discrepancy between the experimental and calculated values of D and E could be explained by a mean field effect between the two asymmetric units we performed similar calculations with unit B. The results do not change by any significant amount (Table 2). The easy ($D < 0$) axis is the locally defined y axis pointing along the Mn–O bond, and the z axis belongs to the axially (Jahn–Teller) distorted Mn–N2 bonds.

The experimentally determined D and E parameters from HF-EPR differ from the calculated by as much as 0.8 and 0.5 cm^{-1} , respectively, based on the best method (NEVPT2 + SOC). Better theoretical values would necessarily require the use of MRCI approaches which for an active space of this size would be computationally prohibitive.

Experimental

General remarks

3-Ethoxysalicylaldehyde, *N*-methyl-1,3-diaminopropane, manganese(II) chloride tetrahydrate, sodium tetraphenylborate, methanol and acetonitrile were purchased and used without further purification. IR spectra were obtained on a Nicolet Nexus 6700 FTIR spectrophotometer in the 400–4000 cm^{-1} range with 4 cm^{-1} resolution using KBr pellets. Microanalyses for C, H and N quantifications were performed at CACTI, University of Vigo (Spain) on a Fisons Carlo Erba EA110.

Complex 1

To a solution of 3-ethoxysalicylaldehyde (0.338 g, 2 mmol) in methanol (10 mL) *N*-methyl-1,3-diaminopropane (0.209 mL, 2 mmol) was added to give a yellow coloured mixture that was stirred at room temperature for 15 min. A solution of manganese(II) chloride tetrahydrate (0.195 g, 1 mmol) and sodium tetraphenylborate (0.341 g, 1 mmol) previously stirred in methanol (10 mL) for 15 min was added to the mixture and left stirring for 1 h. The brown precipitate formed was filtered off and dissolved in acetonitrile (10 mL). Brown crystals were obtained after slow evaporation of the solvent (0.219 g, 26%). IR: $\nu_{\text{max}}/\text{cm}^{-1}$ 3265 ($\nu_{\text{N-H}}$, m), 3053 ($\nu_{\text{C-H}}$, m), 1610 ($\nu_{\text{C=N}}$, s),

Table 2 Calculated ZFS parameters with several approaches

Method	MOLCAS	ORCA	
	CASSCF + SOC		NEVPT2 + SOC
Crystallographic unit A			
D/cm^{-1}	−3.225	−3.054	−3.809
E/cm^{-1}	+0.645	+0.583	+1.046
g_{iso}	1.987	1.987	1.988
Crystallographic unit B			
D/cm^{-1}	−3.224	−3.050	−3.747
E/cm^{-1}	+0.625	+0.565	+0.983
g_{iso}	1.987	1.987	1.988

1595 ($\delta_{\text{C}=\text{C}}$, s), 734 (ν_{BPh_1} , s), 707 (ν_{BPh_2} , s). Anal. found (calcd) for $\text{C}_{50}\text{H}_{58}\text{BMnN}_4\text{O}_4$ (%): $\text{C}_{50}\text{H}_{58}\text{BMnN}_4\text{O}_4$: C 71.02 (71.09); H 7.09 (6.92); N 6.71 (6.63).

General procedures for X-ray crystallography

Crystals suitable for single-crystal X-ray analysis were obtained for complex **1** as described in the synthesis procedure. The data were collected using a graphite monochromated Mo-K α radiation ($\lambda = 0.71073 \text{ \AA}$) on a Bruker AXS-KAPPA APEX II diffractometer equipped with an Oxford Cryosystem open-flow nitrogen cryostat. Cell parameters were retrieved using Bruker SMART software and refined using Bruker SAINT on all observed reflections. Absorption corrections were applied using SADABS.³³ The structures were solved and refined using direct methods with program SIR2004³⁴ using WINGX-Version 2014.1³⁵ SHELXTL³⁶ system of programs. All non-hydrogen atoms were refined anisotropically and the hydrogen atoms were inserted in idealised positions and allowed to refine riding on the parent carbon atom. The molecular diagrams were drawn with ORTEP-3 for Windows⁵ included in the software package.

For crystallographic experimental data and structure refinement parameters see Table S1.† CCDC 1451873 contains the supplementary crystallographic data for this paper.

General procedures for magnetic measurements

The temperature dependence of the magnetisation was measured using a SQUID magnetometer (Quantum Design MPMS) in the temperature range of 10–300 K under a magnetic field of 1000 Oe. The $\chi_{\text{M}}T$ vs. T variation is shown in Fig. S2.†

AC susceptibility measurements were performed using a MagLab 2000 system (Oxford Instruments). The temperature dependence of AC magnetic susceptibility was measured using a 2 Oe oscillating field in the 10–10 000 Hz frequency range under zero and 2000 Oe static fields (Fig. S5†). Additional isothermal AC susceptibility measurements, $\chi_{\text{AC}} = f(\omega)$, were taken in the 10–10 000 Hz frequency range within 1.6 and 4 K (Fig. 4), the temperature range in which the relaxation time reaches a maximum. Cole–Cole plots were fitted using a generalized Debye model,^{37,38} $\chi(\omega) = \chi_{\text{S}} + (\chi_{\text{T}} + \chi_{\text{S}})/(1 + i\omega\tau)^{1-\alpha}$, which describes both real and imaginary components of AC susceptibility, χ' and χ'' in terms of frequency, isothermal susceptibility (χ_{T}), adiabatic susceptibility (χ_{S}), relaxation time (τ), and a variable representing the distribution of relaxation times (α) (Fig. S6†).

High frequency electron paramagnetic resonance

The HF-EPR spectra were recorded on a home-built broadband HF-EPR spectrometer at the University of Stuttgart at frequencies between 180 GHz and 700 GHz (Fig. 3), and in a temperature range from 3 K to 40 K (Fig. S3†), on a 25 mg powdered sample pressed into a 5 mm pellet. Spectra were simulated with the help of the EasySpin program.³⁹

Computational details

The CASSI calculations were performed using the MOLCAS^{40,41} program (version 8.0.14-09-21) with Atomic Natural Orbital Relativistic Core Contracted (ANO-RCC) basis sets possessing the following contraction schemes:

Mn: 6s5p3d2f1g; O/N: 3s2p1d; C: 3s2p; H: 2s

An active space of four electrons in five orbitals CAS(4,5) was chosen for the title complex averaging each spin state over the entire CI space spanning the ligand field orbitals (5 quintet roots, 45 triplet roots and 50 singlet roots). All the roots were used to compute the transition densities in the RASSI module which handles the spin–orbit state interaction. The Atomic Mean Field Integral (AMFI) approximation was used^{42,43} and the Douglas–Kroll–Hess^{44–46} relativistic Hamiltonian was employed to second order (DKH2). No symmetry was used in the calculation. The Cholesky⁴⁷ integral decomposition technique was used as a density fitting procedure in the multi-centre integral routines. The SINGLE_ANISO module⁴⁸ was used to extract the ZFS parameters from the RASSI generated SOC densities. A basis set with more primitives in the contraction scheme was tried for unit A (Mn: 6s5p3d2f1g; O/N/C: 4s3p2d1f; H: 2s1p) and did not yield any improvement in the CASSCF-SO values of D (-3.226 cm^{-1}) and E (0.604 cm^{-1}).

Additionally the ORCA⁴⁹ 3.0.3 program package was used for the calculation of some of the ZFS parameters using an effective Hamiltonian from Quasi-Degenerate Perturbation Theory. The DKH2 Hamiltonian and the ‘chain-of-spheres’ RIJCOSX density fitting⁵⁰ technique were also employed in these calculations. The all electron relativistic basis set re-contractions⁵¹ of Ahlrichs triple zeta⁵² def2-TZVP functions were used for all the atoms. The same CAS space and number of roots were used as in the MOLCAS runs the only difference being that the MO coefficients of all the roots were averaged regardless of the spin state (each with weight of 1/100). The N-Electron Valence Perturbation Theory to second order^{32,53} (NEVPT2) was employed where indicated for perturbative evaluations of the dynamic correlation part, using default parameters and using the state specific canonical CASSCF orbitals.

Conclusions

This work reports the first example of single ion magnetic behaviour found in an *fac*-octahedral Mn(III) complex with two tridentate Schiff-base ligands. Both magnetic measurements and HF-EPR spectroscopy revealed that the size of the axial anisotropy for this Mn(III) single ion magnet is the highest reported to date. The energy barrier for spin reversal (10.19 K) and spin reversal relaxation time ($1.476 \times 10^{-6} \text{ s}$) at 2000 Oe are in agreement with those found for other Mn(III) single ion magnets. Computational studies on complex **1** showed that the easy ($D < 0$) axis is orthogonal to the Jahn–Teller axis. The largest source of this anisotropy is the $t_{2g}^4 e_g^*0$ triplet state which admixes with the quintet ground state. This work opens

a door to investigate other Mn(III) complexes with tridentate Schiff-base ligands.

Acknowledgements

This work was supported by Fundação para a Ciência e a Tecnologia (FCT), Portugal (Projects UID/MULTI/00612/2013, UID/MULTI/04046/2013, UID/QUI/00100/2013 and UID/Multi/04349/2013). FCT is gratefully acknowledged by S. R. for a PhD grant (PD/BD/52368/2013) and by P. N. M. and S. B. for postdoctoral grants (SFRH/BPD/73345/2010 and SFRH/BPD/73941/2010). N. A. G. B. gratefully acknowledges the COFUND 291787-ICIQ-IPMP grant. P. N. and J. S. acknowledge funding from DFG (SPP1601, INST41/863). S. B. is grateful to Centro de Química Estrutural for the access to crystallography facilities. A Science Foundation Ireland Investigator Project Award 12/IP/1703 is gratefully acknowledged by G. G. M. and funding from the National University of Ireland, University College Dublin and the Cultural Service of the French Embassy in Ireland for scholarships is gratefully acknowledged by A. J. F. The COST action CM1305 is acknowledged by P. N. M. and G. G. M.

Notes and references

‡ Crystal data for 1: C₅₀H₅₈BMnN₄O₄; crystal size 0.5 × 0.4 × 0.2 mm; monoclinic system, P₂₁/n space group; a = 12.066(1), b = 18.279(1), c = 20.890(1) Å, α = γ = 90, β = 91.5(0), V = 4605.9(4) Å³. Crystal data collected at 150 K. CCDC 1451873 contains the supplementary crystallographic data for this paper.

- R. Sessoli, D. Gatteschi, A. Caneschi and M. A. Novak, *Nature*, 1993, **365**, 141–143.
- D. Gatteschi, R. Sessoli and J. Villain, *Molecular Nanomagnets*, 2007.
- D. E. Freedman, W. H. Harman, T. D. Harris, G. J. Long, C. J. Chang and J. R. Long, *J. Am. Chem. Soc.*, 2010, **132**, 1224–1225.
- J. M. Zadrozny, M. Atanasov, A. M. Bryan, C.-Y. Lin, B. D. Reinken, P. P. Power, F. Neese and J. R. Long, *Chem. Sci.*, 2013, **4**, 125–138.
- P. P. Samuel, K. C. Mondal, N. Amin Sk, H. W. Roesky, E. Carl, R. Neufeld, D. Stalke, S. Demeshko, F. Meyer, L. Ungur, L. F. Chibotaru, J. Christian, V. Ramachandran, J. van Tol and N. S. Dalal, *J. Am. Chem. Soc.*, 2014, **136**, 11964–11971.
- S. Mossin, B. L. Tran, D. Adhikari, M. Pink, F. W. Heinemann, J. Sutter, R. K. Szilagyi, K. Meyer and D. J. Mindiola, *J. Am. Chem. Soc.*, 2012, **134**, 13651–13661.
- Y. Rechkemmer, F. D. Breitgoff, M. van der Meer, M. Atanasov, M. Hakl, M. Orlita, P. Neugebauer, F. Neese, B. Sarkar and J. van Slageren, *Nat. Commun.*, 2016, **7**, 10467.
- J. Vallejo, A. Pascual-Álvarez, J. Cano, I. Castro, M. Julve, F. Lloret, J. Krzystek, G. De Munno, D. Armentano, W. Wernsdorfer, R. Ruiz-García and E. Pardo, *Angew. Chem., Int. Ed.*, 2013, **52**, 14075–14079.
- R. C. Poulten, M. J. Page, A. G. Algarra, J. J. Le Roy, I. López, E. Carter, A. Llobet, S. A. Macgregor, M. F. Mahon, D. M. Murphy, M. Murugesu and M. K. Whittlesey, *J. Am. Chem. Soc.*, 2013, **135**, 13640–13643.
- K. E. R. Marriott, L. Bhaskaran, C. Wilson, M. Medarde, S. T. Ochsenbein, S. Hill and M. Murrie, *Chem. Sci.*, 2015, **6**, 6823–6828.
- H. L. C. Feltham and S. Brooker, *Coord. Chem. Rev.*, 2014, **276**, 1–33.
- J. Cirera, E. Ruiz, S. Alvarez, F. Neese and J. Kortus, *Chem. – Eur. J.*, 2009, **15**, 4078–4087.
- S. Gómez-Coca, D. Aravena, R. Morales and E. Ruiz, *Coord. Chem. Rev.*, 2015, **289–290**, 379–392.
- H. A. Jahn and E. Teller, *Proc. R. Soc. London, Ser. A*, 1937, **161**, 220–235.
- D. V. Behere and S. Mitra, *Inorg. Chem.*, 1980, **19**, 992–995.
- B. J. Kennedy and K. S. Murray, *Inorg. Chem.*, 1985, **24**, 1552–1557.
- J. Limburg, J. S. Vrettos, R. H. Crabtree, G. W. Brudvig, J. C. de Paula, A. Hassan, A.-L. Barra, C. Duboc-Toia and M.-N. Collomb, *Inorg. Chem.*, 2001, **40**, 1698–1703.
- C. Mantel, A. K. Hassan, J. Pécaut, A. Deronzier, M.-N. Collomb and C. Duboc-Toia, *J. Am. Chem. Soc.*, 2003, **125**, 12337–12344.
- R. Ishikawa, R. Miyamoto, H. Nojiri, B. K. Breedlove and M. Yamashita, *Inorg. Chem.*, 2013, **52**, 8300–8302.
- A. Grigoropoulos, M. Pissas, P. Papatolis, V. Psycharis, P. Kyritsis and Y. Sanakis, *Inorg. Chem.*, 2013, **52**, 12869–12871.
- G. A. Craig, J. J. Marbey, S. Hill, O. Roubeau, S. Parsons and M. Murrie, *Inorg. Chem.*, 2015, **54**, 13–15.
- A. Pascual-Álvarez, J. Vallejo, E. Pardo, M. Julve, F. Lloret, J. Krzystek, D. Armentano, W. Wernsdorfer and J. Cano, *Chem. – Eur. J.*, 2015, 17299–17307.
- A search using CCDC Conquest program returned 64 hits with the following bond distance ranges: Mn(III)–O_{phenolate} 1.850–1.902 Å, M(III)–N_{amine} 2.031–2.389 Å, Mn(III)–N_{imine} 1.975–2.159 Å. See for example: B. Gildea, M. M. Harris, L. C. Gavin, C. A. Murray, Y. Ortin, H. Müller-Bunz, C. J. Harding, Y. Lan, A. K. Powell and G. G. Morgan, *Inorg. Chem.*, 2014, **53**, 6022–6033.
- N. F. Chilton, R. P. Anderson, L. D. Turner, A. Soncini and K. S. Murray, *J. Comput. Chem.*, 2013, **34**, 1164–1175.
- D. Gatteschi and R. Sessoli, *Angew. Chem., Int. Ed.*, 2003, **42**, 268–297.
- W. H. Harman, T. D. Harris, D. E. Freedman, H. Fong, A. Chang, J. D. Rinehart, A. Ozarowski, M. T. Sougrati, F. Grandjean, G. J. Long, J. R. Long and C. J. Chang, *J. Am. Chem. Soc.*, 2010, **132**, 18115–18126.
- R. Maurice, K. Sivalingam, D. Ganyushin, N. Guihéry, C. de Graaf and F. Neese, *Inorg. Chem.*, 2011, **50**, 6229–6236.
- J. Long, F. Habib, P.-H. Lin, I. Korobkov, G. Enright, L. Ungur, W. Wernsdorfer, L. F. Chibotaru and M. Murugesu, *J. Am. Chem. Soc.*, 2011, **133**, 5319–5328.

- 29 R. J. Blagg, L. Ungur, F. Tuna, J. Speak, P. Comar, D. Collison, W. Wernsdorfer, E. J. L. McInnes, L. F. Chibotaru and R. E. P. Winpenny, *Nat. Chem.*, 2013, **5**, 673–678.
- 30 In an attempt to improve the calculated ZFS parameters we explored the possibility of non-local dynamic correlation playing a role. With the MOLCAS program this can be accomplished *via* the CASPT2 method but unfortunately this entails solving a set of linear equations iteratively for each of the 100 states resulting in an unrealistically lengthy calculation. This effort would further be compounded with convergence problems and intruder states for the higher lying excitations.
- 31 C. Duboc, D. Ganyushin, K. Sivalingam, M.-N. Collomb and F. Neese, *J. Phys. Chem. A*, 2010, **114**, 10750–10758.
- 32 C. Angeli, R. Cimiraglia, S. Evangelisti, T. Leininger and J.-P. Malrieu, *J. Chem. Phys.*, 2001, **114**, 10252.
- 33 G. M. Sheldrick, *SADABS, Empirical Absorpt. Correct. program*, Univ. Göttingen, 1995, based on the methods of Blessing.
- 34 M. C. Burla, R. Caliendo, M. Camalli, B. Carrozzini, G. L. Cascarano, L. De Caro, C. Giacovazzo, G. Polidori and R. Spagna, *J. Appl. Crystallogr.*, 2005, **38**, 381–388.
- 35 L. J. Farrugia, *J. Appl. Crystallogr.*, 1999, **32**, 837–838.
- 36 G. M. Sheldrick, *Acta Crystallogr., Sect. A: Fundam. Crystallogr.*, 2008, **64**, 112–122.
- 37 K. S. Cole and R. H. Cole, *J. Chem. Phys.*, 1941, **9**, 341.
- 38 S. M. J. Aubin, Z. Sun, L. Pardi, J. Krzystek, K. Folting, L.-C. Brunel, A. L. Rheingold, G. Christou and D. N. Hendrickson, *Inorg. Chem.*, 1999, **38**, 5329–5340.
- 39 S. Stoll and A. Schweiger, *J. Magn. Reson.*, 2006, **178**, 42–55.
- 40 K. Andersson, M. Barysz, A. Bernhardsson, M. R. A. Blomberg, Y. Carissan, D. L. Cooper, M. Cossi, A. Devarajan, M. P. Fülscher, A. Gaenko, L. Gagliardi, C. De Graaf, B. A. Hess, D. Hagberg, G. Karlström, J. W. Krogh, R. Lindh, P.-Å. Malmqvist, T. Nakajima, P. Neogrady, J. Olsen, T. B. Pedersen, J. Raab, B. O. Roos, U. Ryde, B. Schimmelpfennig, M. Schütz, L. Seijo, L. Serrano-Andrés, P. E. M. Siegbahn, J. Stålring, T. Thorsteinsson, V. Veryazov and P.-O. Widmark, <http://www.teokem.lu.se/molcas>.
- 41 F. Aquilante, L. De Vico, N. Ferré, G. Ghigo, P. A. Malmqvist, P. Neogrady, T. B. Pedersen, M. Pitonák, M. Reiher, B. O. Roos, L. Serrano-Andrés, M. Urban, V. Veryazov and R. Lindh, *J. Comput. Chem.*, 2010, **31**, 224–247.
- 42 B. A. Hess, C. M. Marian, U. Wahlgren and O. Gropen, *Chem. Phys. Lett.*, 1996, **251**, 365–371.
- 43 P. A. Malmqvist, B. O. Roos and B. Schimmelpfennig, *Chem. Phys. Lett.*, 2002, **357**, 230–240.
- 44 M. Douglas and N. M. Kroll, *Ann. Phys.*, 1974, **82**, 89–155.
- 45 B. A. Hess, *Phys. Rev. A*, 1986, **33**, 3742–3748.
- 46 G. Jansen and B. A. Hess, *Phys. Rev. A*, 1989, **39**, 6016–6017.
- 47 F. Aquilante, T. B. Pedersen, R. Lindh, B. O. Roos, A. Sánchez de Merás and H. Koch, *J. Chem. Phys.*, 2008, **129**, 024113.
- 48 L. F. Chibotaru and L. Ungur, *J. Chem. Phys.*, 2012, **137**, 064112.
- 49 F. Neese, *WIREs Comput. Mol. Sci.*, 2012, **2**, 73–78.
- 50 F. Neese, F. Wennmohs, A. Hansen and U. Becker, *Chem. Phys.*, 2009, **356**, 98–109.
- 51 D. A. Pantazis, X.-Y. Chen, C. R. Landis and F. Neese, *J. Chem. Theory Comput.*, 2008, **4**, 908–919.
- 52 A. Schäfer, C. Huber and R. Ahlrichs, *J. Chem. Phys.*, 1994, **100**, 5829.
- 53 C. Angeli, R. Cimiraglia and J.-P. Malrieu, *Chem. Phys. Lett.*, 2001, **350**, 297–305.